01 Jan 1978

# PERFORMANCE of a DUAL-RANGE CLOUD NUCLEUS COUNTER.

Darryl J. Alofs
*Missouri University of Science and Technology*, dalofs@mst.edu



## Recommended Citation

D. J. Alofs, "PERFORMANCE of a DUAL-RANGE CLOUD NUCLEUS COUNTER.," *Journal of Applied Meteorology*, vol. 17, no. 9, pp. 1286 - 1297, American Meteorological Society, Jan 1978.
The definitive version is available at https://doi.org/10.1175/1520-0450(1978)017<1286:POADRC>2.0.CO;2

# Performance of a Dual-Range Cloud Nucleus Counter

DARRYL J. ALOFS

*Department of Mechanical Engineering and Cloud Physics Research Center, University of Missouri, Rolla 65401*

(Manuscript received 30 November 1977, in final form 15 April 1978)

ABSTRACT

An instrument for measuring the concentrations of cloud condensation nuclei as a function of nucleus critical supersaturation ($S_c$) is described. In the range $0.1\% \leqslant S_c \leqslant 1\%$, the instrument is operated as a vertical flow thermal diffusion chamber. In the range $0.016\% \leqslant S_c \leqslant 0.1\%$, the chamber is operated at 100% humidity, and the equilibrium radii of the nuclei are measured with an optical counter. This paper presents a large body of data taken in the laboratory to evaluate the performance of the instrument. The data indicates that the instrument is internally consistent over a wide range of operating conditions.

## 1. Introduction

For two decades the horizontal-plate, static thermal diffusion chamber has been the most widely used instrument for measuring cloud condensation nuclei (CCN) concentrations. Long ago Twomey (1967) recognized that this instrument should not be used below a supersaturation $S$ of 0.1%. The problem at lower supersaturations is that very large growth times are required before the active nuclei grow large enough to be distinguished from the unactivated nuclei. Hoppel and Wojciechowski (1976) presented experimental evidence that even at $S=0.2\%$, the instrument was sometimes unsatisfactory. Shortly thereafter, Alofs and Carstens (1976) presented a numerical simulation of the instrument which showed surprisingly large error estimates.

There have been a series of efforts to develop more accurate CCN counters. Laktionov (1965, 1968) utilized an optical counter to count the water drops grown on the nuclei. In comparison to the photographic method of counting droplets, this allowed better discrimination of which size droplets were being counted. This then improved the ability to distinguish haze drops from those grown on active nuclei. Laktionov also recognized the advantage of increasing the growth time experienced by the nuclei. In 1968 he used a vertical thermal diffusion chamber consisting of concentric vertical cylinders. This allowed the nuclei to experience increased growth time and hence made it easier to distinguish haze drops from active drops. Although Laktionov was innovative in the above two respects, he did not analyze the effects of convection currents in his vertical instrument and it was criticized on that account (Saxena and Carstens, 1971).

Laktionov (1972) then developed an entirely different type of cloud nucleus counter which he called the isothermal cloud nucleus counter. At that time he showed that after measuring the equilibrium size of a nucleus at 100% humidity, the critical supersaturation $S_c$ of the nucleus could be calculated rather accurately, without knowing very much about the chemical composition of the nucleus. This is in contrast to the need for extensive chemical composition knowledge when trying to predict $S_c$ from a measurement of nucleus dry size. In Laktionov's instrument, the nuclei pass through a humidification tube, in which they experience 100% relative humidity, and then the nuclei are counted according to size as they pass through an optical counter. A brief review (Alofs and Podzimek, 1974) of Laktionov's paper was published as a result of a personal meeting between Laktionov and Alofs in Leningrad. However, prior to 1974, Laktionov's paper did not receive much attention and efforts to develop improved CCN counters were focused mainly on thermal diffusion chambers.

Hudson and Squires (1973) described a horizontal-plate, steady-flow thermal diffusion chamber which utilized an optical counter. It featured a dry region on the hot plate to avoid the transient supersaturations described by Fitzgerald (1970) and by Saxena *et al.* (1970). It also featured a filtered air sheath system designed so that nuclei passed through the chamber in a narrow stream located at the chamber midplane, with filtered air occupying the spaces near the chamber walls. This meant that only nuclei experiencing a uniform supersaturation were counted, even though all of the volume flow through the chamber went into the optical counter. As shown later in this paper, large flow rates into the optical counter minimize otherwise troublesome problems of droplet evaporation. The performance of the Hudson–Squires instrument was very impressive because the optical counter showed quantitatively the decrease in the water droplet monodispersity as the growth time was decreased. However, the lowest supersaturation tested was 0.5%.

0021-8952/78/1286-1297$06.00

Shortly after this, Sinnarwalla and Alofs (1973) described a vertical thermal diffusion chamber in which the sample flowed downward between vertical plates. They investigated the effect of convection currents and found that convection did not influence the nuclei supersaturation histories if the net downward flow was sufficiently large. They also found that thermophoretic and diffusiophoretic forces placed a significant limitation on the available growth time. The chamber was equipped both for photographic drop counting and also *in situ* photoelectric drop counting. The latter technique was abandoned in 1974 because the maximum counting rate was 5 drops per minute.

A more successful vertical-plate thermal diffusion chamber was described by Hudson and Squires (1976). Their instrument featured horizontal flow between vertical plates, rather than vertical flow as in the Sinnarwalla–Alofs chamber. They showed that this vertical chamber agreed with their horizontal chamber to within 1% accuracy over the supersaturation range 1–0.25%. They also showed that their vertical chamber could be used at lower supersaturations then their horizontal chamber, however, even the vertical chamber performance deteriorated significantly at 0.08% supersaturation.

Hudson *et al.* 1977 described experiments in which the Hudson–Squires horizontal flow instrument and a static instrument were intercompared. It was found that the two instruments agreed to within 20% accuracy over the supersaturation range 0.25–1%. This is surprisingly good agreement in view of the numerical simulation of Alofs and Carstens (1976). Since the static thermal diffusion chambers are generally smaller and simpler than steady-flow thermal diffusion chambers, they have advantages, especially for some field measurements. Therefore the above disagreement between theory and experiment should be investigated further.

We now describe the instrument whose performance data are presented in this paper. The instrument operates in two modes. For the range $0.1\% < S_c < 1\%$, the instrument operates as a vertical flow thermal diffusion chamber; for the range $0.016\% < S_c < 0.1\%$, it operates as an isothermal chamber. In both modes, an optical counter is used to size the water drops coming out of the chamber. Most of the performance tests in the isothermal mode go beyond the tests published by Laktionov for his isothermal chamber. About half of the performance tests in the thermal diffusion mode were performed by Hudson and Squires (1976) for their instruments.

## 2. The chamber

Fig. 1 is a schematic of the chamber. The sample air enters at the top, passing through a tube 0.5 mm diameter by 6 cm long and then through a tube 0.25 mm diameter by 2.5 cm long. These two tubes are coaxial,

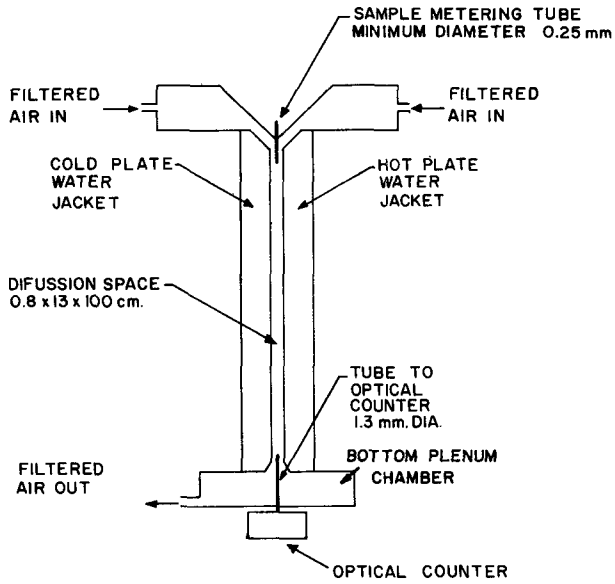


FIG. 1. Schematic of the chamber.

and are positioned as shown in Fig. 1, where they are labeled as the sample metering tube. The pressure drop across the sample metering tube meters the sample flow rate, which is usually in the range 4–16 $cm^3\ min^{-1}$. Filtered air also enters the chamber at the top, through the wing-shaped portions of the chamber (Fig. 1), which are filled with 1 mm diameter glass beads to break up the larger vortices. The sample air blends with the filtered air and flows down between the parallel plates in such a way that the sample air remains midway between the plates in a narrow coherent stream. This flow pattern was successfully achieved only after some trial and error modifications of the inlet design. For example, originally the sample metering tube was only 2.5 cm long, so that the sample emerged from the tube within the region where the filtered air was still making its downward turn from the left and right wings. With this arrangement the aerosol stream did not remain as coherent as with the present design. Likewise, the glass beads were found to improve the coherence of the aerosol stream. In all cases, the evidence for improved coherence was improved monodispersity of the water droplet size distribution from the optical counter, as discussed further in Section 5.

The parallel plates together with the rubber side walls enclose a rectangular space 100 cm long in the vertical direction, with a 0.8 cm by 13 cm rectangular cross section. Each plate is constructed of a piece of rectangular aluminum tube of 3 mm wall thickness through which thermostated water flows at a rate of 30 $\ell\ min^{-1}$ to keep each plate isothermal. When operated as a thermal diffusion chamber, one plate is kept hotter than the other, and the inside surfaces of each plate are covered with filter paper continuously saturated with water. In order to avoid transient super-

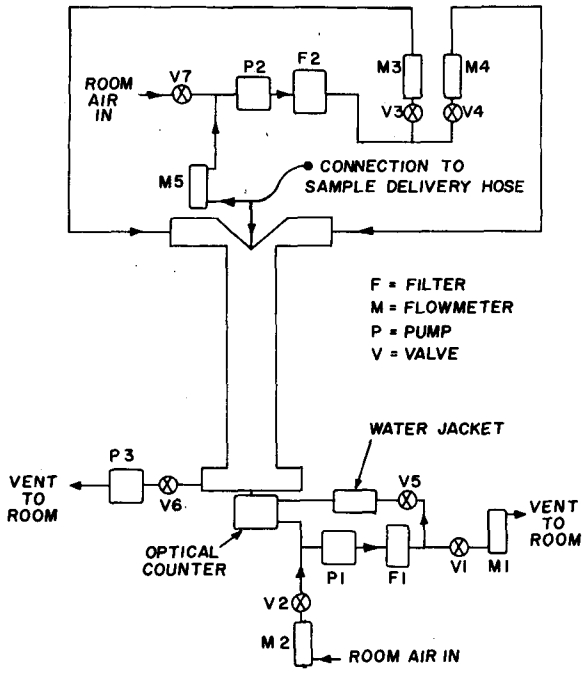


FIG. 2. The external air flow systems.

saturations, the top 15 cm of the hot plate is kept dry (Mahata *et al.*, 1973).

The development of the temperature and vapor pressure profiles in the entrance region of the chamber has been analyzed by Mahata *et al.* (1973). This analysis shows that the profiles are fully developed within a length of 3 to 20 cm for filtered air flow rates between 0.2 and 5 $\ell$ min$^{-1}$, respectively. Downstream of this length there are no gradients in the flow direction, while both temperature and vapor pressure decrease linearly with distance from the hot plate. This produces a supersaturation profile of approximately parabolic distribution, with the maximum or operating supersaturation midway between the plates, and saturation at the plates.

At the bottom of the chamber, where water drops have grown on the active nuclei, the sample air plus some of the filtered air is sucked into the optical counter through a tube 1.3 mm diameter by 12 cm long. The largest portion of the filtered air, however, does not go into this tube, but instead flows down past it into a bottom plenum chamber (Fig. 1). It was found that this design causes the crossover region of the convection loop to move down into the bottom plenum chamber, as discussed in Section 4.

## 3. The external air flow systems

Fig. 2 shows the air flow systems external to the chamber. The system at the top of Fig. 2 takes ambient air, filters it, and introduces a measured flow into each wing of the chamber. This system also sucks sample air through a sample delivery hose at a large enough flow rate (2 $\ell$ min$^{-1}$) so that diffusional losses are negligible. The sample metering tube is connected to a 0.5 mm hole in the wall of this sample delivery hose.

The system at the bottom right corner of Fig. 2 is associated with the optical counter. There are two air flows into the optical counter and one air flow out of it. One inflow is through the 1.3 mm tube (Fig. 1), which extends to within about 1 mm of the top edge of the light beam. The other inflow is the so called sheath air, which is a large (30 $\ell$ min$^{-1}$) flow of filtered air for the purpose of purging the optical chamber and minimizing the deposition of stray aerosol particles on the optics. The sheath air enters the optical chamber at the same place as the 1.3 mm tube, through a 6 mm tube which is coaxial with the 1.3 mm tube and which likewise reaches to within 1 mm of the light beam. These two airflows both pass through the light beam and then flow out of the optical chamber.

The temperature of the sheath air influences the temperature of the 1.3 mm tube, and hence influences possible evaporation of the water drops passing through it. Since the sheath air pump heats the sheath air considerably, provisions described in Section 6 are made to cool it before it enters the optical chamber. The humidity of the sheath air also has some influence on droplet evaporation, but only during the time it takes for a droplet to traverse the distance from the exit end of the 1.3 mm tube to the light beam. The control of sheath air humidity is discussed next.

It can be seen from Fig. 2 that room air is sucked into the optical counter flow loop. This is necessary because otherwise the steady-state dew point of the sheath air would equal the dew point of the air being sucked in through the 1.3 mm tube. This would cause condensation on the optics unless they were heated, which is also undesireable. With the arrangement in Fig. 2, the steady-state humidity of the sheath air is a weighted average of the room humidity and the humidity of the air being sucked into the 1.3 mm diameter tube, the weighing factor for each being proportional to the respective flow. Thus the humidity of the sheath air can be controlled. Generally, it is kept at 60–70%.

It is necessary to accurately measure the flow being sucked into the Royco through the 1.3 mm tube. This flow is called the Royco flow, and it ranges from 0.2 to 3 $\ell$ min$^{-1}$. Since the sheath air flow is so much larger than this, it would be inaccurate to measure the Royco flow by taking the difference between measured flow out of the Royco and the sheath flow into the Royco. Instead, we measure the Royco flow by taking the difference between flowmeters 1 and 2 in Fig. 2. Pump 1 is a metal bellows pump with virtually zero leakage so this may be done accurately.

The system at the bottom left corner of Fig. 2 sucks filtered air out of the bottom plenum of the chamber. In total, then, there are three external air flow systems, each with its own pump, so that adjusting the values

in one system does not greatly influence the flows in the other systems.

## 4. Convection effects

Experimental and theoretical investigations of the convection effects in the chamber were presented by Sinnarwalla and Alofs (1973). The reader is referred to this source for more details, but briefly, the flow field consists of the forced convection field superimposed on the free convection field. The forced convection field is due to the net downward flow being forced by the pump sucking at the bottom of the chamber. This produces a parabolic velocity profile between the plates, with a maximum downward velocity midway between the plates. The free convection field is caused by buoyancy forces due to the horizontal temperature gradient in the chamber. The free convection component of the velocity field is therefore a circulation, giving upward velocity near the hot plate and downward velocity near the cold plate. At the top of the chamber there is a horizontal crossover velocity toward the cold plate and at the bottom of the chamber there is a horizontal crossover velocity toward the hot plate.

It is necessary that the water drops be counted before they pass through the bottom crossover region, because otherwise some water droplets could be recirculated in the chamber and also because transient supersaturations occur in the bottom crossover region (Saxena and Carstens, 1971). The present design achieves this because it was found that if enough of the filtered air is pulled into the bottom plenum of the chamber (Fig. 1) then the crossover region occurs in the bottom plenum, and hence does not influence the water droplets.

The evidence as to position of the crossover region was obtained by watching the drop sizes going through the optical counter. When the water droplets were all the same size, this was evidence that all the nuclei were experiencing the same supersaturation, whereas when the drops passed through the crossover region, some of them were recirculated and there was a bimodal size distribution of water drops. This could be seen quite clearly on an oscilloscope connected to the preamp output from the phototube of the optical counter. With the oscilloscope set at a sweep rate of 10 ms, the pulses from at least 50 water drops could be viewed in one sweep. The degree of water drop monodispersity achieved is discussed in the next section.

## 5. Aerosol stream diameter and position

Since the fully developed velocity profile in the chamber is parabolic (Mahata *et al.*, 1973), the velocity at the midplane to the chamber is 1.5 $Q/A$, where $Q$ is the total volume flow rate in the chamber and $A$ the cross-sectional area of the chamber ($=10.4$ cm$^2$). A narrow aerosol stream located at the midplane of the chamber has this same velocity, and equals $4q/\pi d^2$, where $d$ is the diameter and $q$ is the volume flow rate of the aerosol stream. Setting these velocities equal gives

$$d=(0.849qA/Q)^{\frac{1}{2}}. \quad (1)$$

For the experiments described below, the values for $q$ and $Q$ are 8.5 cm$^3$ min$^{-1}$ and 8 $\ell$ min$^{-1}$, respectively, for which Eq. (1) then gives $d=0.1$ cm. This does not take into account any mixing between the aerosol stream and the surrounding filtered air.

To experimentally investigate the size and position of the aerosol stream, we utilized the fact that a necessary condition for growing a monodisperse cloud of drops is that all the nuclei must experience the same supersaturation $S$. Another necessary condition is that the drops be grown large enough so that the influence of a polydisperse nuclei distribution is left behind; at $S=1.0$ and $S=0.6\%$ a $Q$ of 8 $\ell$ min$^{-1}$ gives sufficiently long growth time for this.

For these conditions and using room air as the test aerosol, we observed that about 90% of the pulses on the oscilloscope had the same pulse height to within an accuracy of 16%. According to the response curve for the optical counter, this corresponds to about an 8% variation in droplet size. Since drop growth is approximately proportional to $S^{\frac{1}{2}}$, these drops could not have experienced a variation in $S$ larger than 16%. Utilizing the fact that the spatial distribution of $S$ is approximately parabolic (Squires, 1972), one can calculate that the nuclei had to be located within 0.16 cm of the midplane of the chamber for most of their residence time in the chamber. This is evidence that the aerosol stream remains very coherent and centered between the plates.

Because of the need to grow large enough drops to leave behind the effect of the polydisperse nuclei distribution, this test could not be run over the entire useful range of the chamber operating parameters. However, such tests are planned in the future using a monodisperse salt aerosol.

## 6. Droplet shrinkage in the optical counter

The water drops are sized according to how much light they scatter as they pass through a beam of light in a Royco Model 225 optical counter, equipped with the 5-channel Royco Model 518 pulse height discriminator[1]. Of major concern is evaporation shrinkage of the drops before they reach the light beam. This shrinkage depends upon the temperature of the 1.3 mm diameter tube (Fig. 1) which is kept warmer than the dew point of the air in the tube. The reason the tube is kept warmer is that otherwise water condenses in the tube and within a short time is sprayed out into the optics of the counter rendering it temporarily inoperable. The optical counter then can be made operable again by flowing dry filtered air through it,

[1] Royco Instruments, Menlo Park, CA.

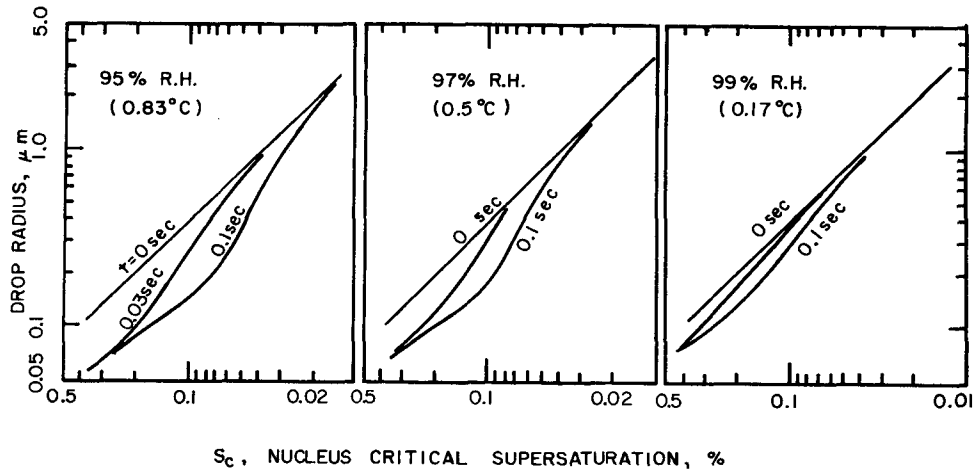


FIG. 3. Theoretical results for droplet evaporation in 1.3 mm tube at 0.2 $\ell$ min$^{-1}$ Royco flow.

but some water spots are left on the lenses and so the damage is not entirely reversible.

When the chamber is being used in the thermal diffusion mode at high supersaturations, the drops can be grown large enough so that evaporation shrinkage is not significant; in addition, the optical counter is then being used mainly to count the drops rather than discriminate their size. At lower supersaturations, size discriminations become relatively more important, and in the isothermal mode one is relying entirely on drop size measurement to determine nucleus critical supersaturation.

At the lowest flow rates into the optical counter the problem of drop evaporation is most severe, so we performed theoretical calculations of droplet evaporation for our lowest flow into the optical counter, which is 0.2 $\ell$ min$^{-1}$. Since the velocity profile in the 1.3 mm tube is parabolic, the droplets at the center of the tube pass through it more quickly than those near the wall of the tube. One can calculate that at 0.2 $\ell$ min$^{-1}$, 80% of the droplets passing through the tube have residence times in the range 0.03–0.10 s. The calculations of droplet shrinkage were performed using the theory and values for thermophysical properties described in an earlier paper (Alofs and Carstens, 1976). The results are shown in Fig. 3 for tube temperatures of 0.83, 0.5 and 0.17°C warmer than the isothermal chamber temperature. The abscissa shows the nucleus critical supersaturation $S_c$ and the ordinate the radius of the nucleus. The line marked $t=0$ designates the condition at the time the nucleus enters the tube where its radius is $r_{100}$, the equilibrium radius at 100% humidity. The lines marked $t=0.03$ s and $t=0.1$ s show the radius of the nucleus as it leaves the tube. It can be seen that for nuclei with $S_c>0.1\%$, evaporation is an overwhelming problem. For nuclei with $0.01\%<S_c<0.1\%$, it can be seen that evaporation will be relatively insignificant only if the tube temperature can be thermostatted to within an accuracy of about 0.1°C.

The provisions made for thermostatting the optical counter are fourfold. First, a flat aluminum plate with water passages through it is mounted onto the bottom of the optical bench, which is also made of aluminum. This plate is the same size as the optical bench, so that the entire flat bottom surface of the optical bench is in contact with this flat plate, while the optical components bolt down directly to the top surface of the optical bench. Water from a thermostated thermal bath, called the Royco thermal bath, is circulated through this flat plate. Second, 30 l min$^{-1}$ of filtered air is pumped through 3 m of 1 cm diameter copper tubing immersed in the Royco thermal bath, and then passed over the optics, but inside a sheet metal cover which is commercially provided for the optics. Third, water from the Royco thermal bath is pumped through an air-water heat exchanger equipped with a fan which forces and recirculates thermostatted air through a plywood box surrounding the optical counter. Fourth, the Royco sheath air passes through 6 m of 1 cm diameter copper tubing immersed in the Royco thermal bath before it goes into the optics. These four provisions are used simultaneously to control the temperature of the optical bench.

Since it would be very difficult to measure the temperature of the inside surface of the 1.3 mm diameter tube, we tested for evaporation in the tube by holding the tube temperature constant and varying the dew point of the air going into the tube. Fig. 4 shows results from such an experiment. The chamber was operating in the isothermal mode, with a flow of 0.35 $\ell$ min$^{-1}$ into the Royco, and with the entire flow through the chamber going into the Royco. The temperature of the Royco thermal bath was kept constant at 27.1°C. The values of chamber temperature are shown on the abscissa, this temperature being the only parameter which was varied during the experiment. The concentration of droplets larger than the indicated size thresholds are shown on the ordinate. Room air in a 13 m$^3$ storage tank was the test aerosol.

It can be seen from Fig. 4 that as the chamber temperature increases, the count from the smaller size channels goes up and then levels off. The data indicates that at chamber temperatures above 27.5°C, the drops are no longer evaporating; hence the temperature of the 1.3 mm tube must be 27.5°C even though the Royco bath is at 27.1°C. The experiment was repeated with various room temperatures over a 10°C spread and it was found that the 1.3 mm tube was always about 0.4°C warmer than the Royco bath. As a consequence we normally set the Royco bath to be 0.3°C below the dew point of the air going into the Royco, that is, with the 1.3 mm tube about 0.1°C above this dew point. This choice of standard operating point corresponds to a chamber temperature of 27.4°C in Fig. 4.

The regions of higher temperature in Fig. 4 cannot be used for continuous operation because of condensation in the 1.3 mm tube. We obtained the data in this region of Fig. 4 by an intermittent procedure in which the 1.3 m tube is dried out about once every 5 min by backflowing dry air through it. One last comment about Fig. 4 is that due to the polydispersity of the nuclei, we cannot precisely compare these experimental results to the theoretical results of Fig. 3.

In order to further test the influence of evaporation in the 1.3 mm tube, it was felt desirable to vary the flow into the Royco. In doing this, however, a complication arises because the Royco exhibits a size calibration shift as the Royco flow is varied. This is because the voltage gain in the Royco electronics is somewhat sensitive to the duration of the pulse coming from the phototube. Pulse duration in turn is a function of flow into the Royco. We solved this problem by using polystyrene latex aerosols to determine a schedule for altering the phototube voltage to compensate for this

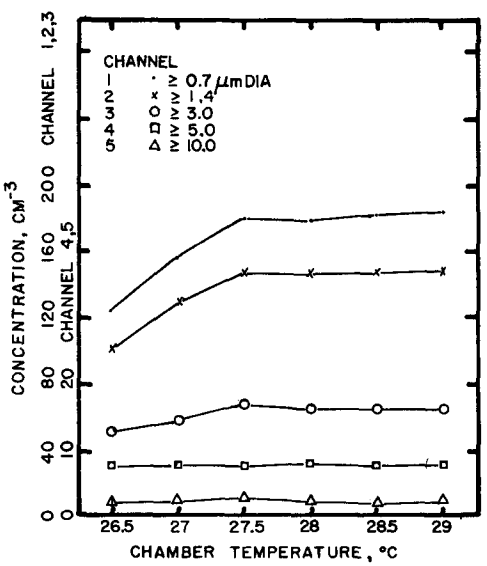


FIG. 4. Test for droplet evaporation with Royco bath held constant at 27.1°C. Royco flow and total flow = 0.35 $\ell$ min$^{-1}$.

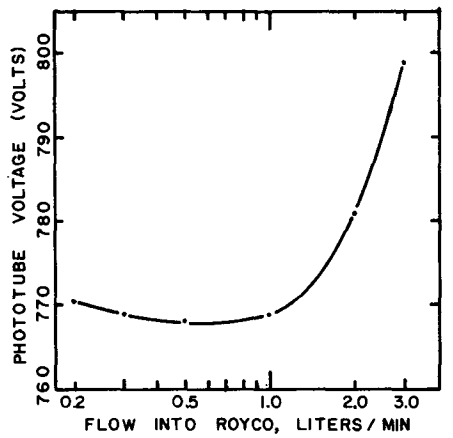


FIG. 5. Voltage schedule to correct for pulse duration sensitivity in Royco electronics.

effect. The resulting schedule is shown in Fig. 5. Data were not taken below 0.2 $\ell$ min$^{-1}$, because it was found that the electronics begins to not count some of the pulses.

Fig. 6 shows results for varying the flow rate of water drops into the Royco, while following the high-voltage schedule of Fig. 5. In this test the isothermal chamber was kept at 27.5°C, and the Royco bath at 27.2°C. Thus the 1.3 mm tube was 0.1°C above the dew point. The total flow through the chamber was 4 $\ell$ min$^{-1}$ and the sample flow was 8.5 cm$^3$ min$^{-1}$. It can be seen from Fig. 6 that the concentration of the small droplets doesn't change even though the residence time in the 1.3 mm tube is varied by more than a factor of

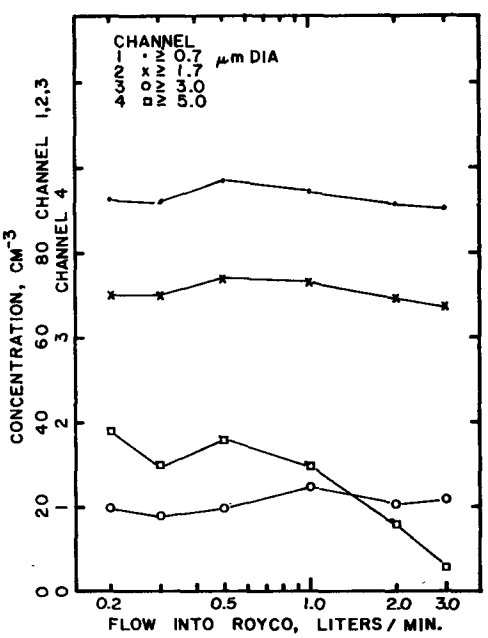


FIG. 6. Test for droplet evaporation: chamber temperature = 27.5°C, Royco bath temperature = 27.2°C, total chamber flow = 4 $\ell$ min$^{-1}$.

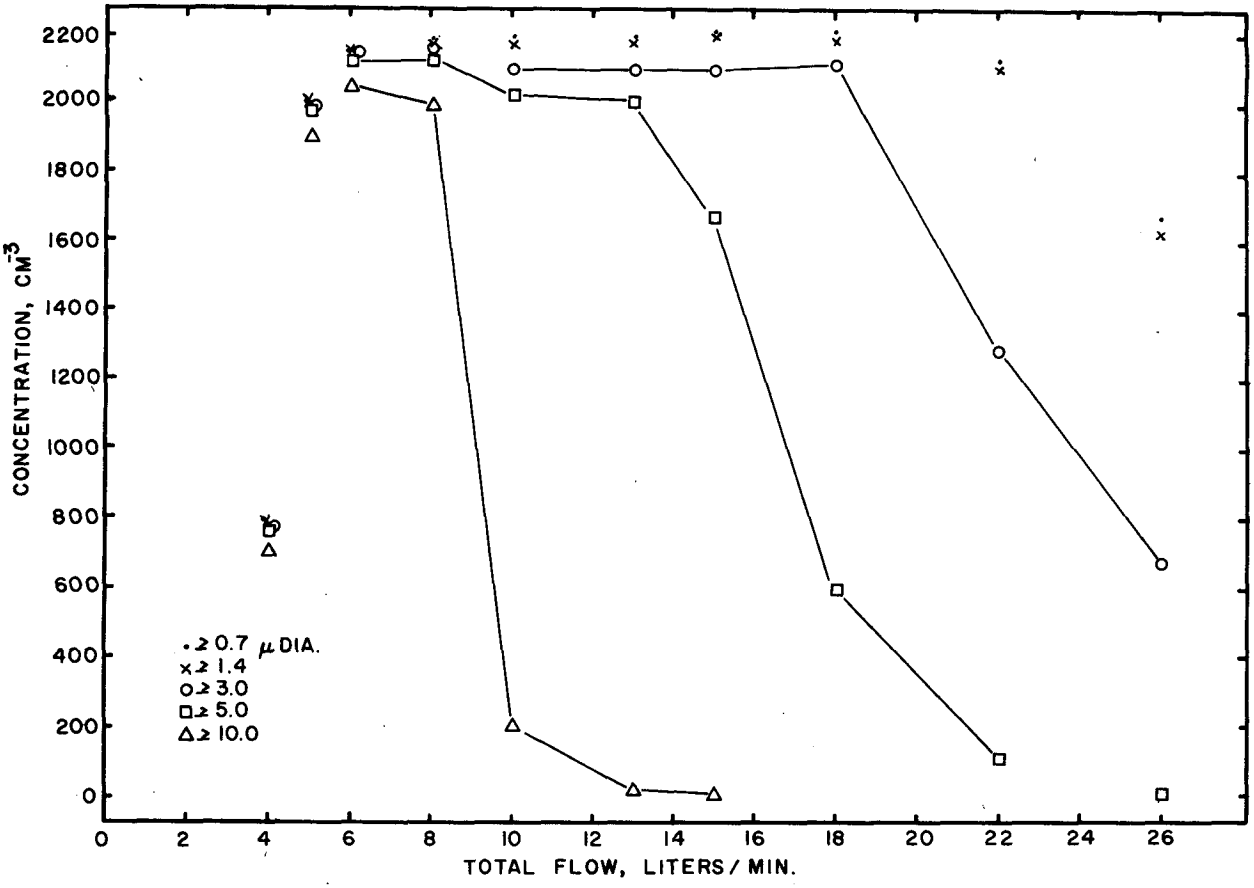


FIG. 7. Cummulative size distribution versus total flow: sample flow = 8.5 cm³ min⁻¹, Royco flow = 0.4 ℓ min⁻¹, supersaturation = 1%.

10. Thus droplet evaporation is negligible. As to the decrease in the largest droplets (channel 4) at higher flow rates, we suspect it is due to impaction at the entrance to the 1.3 mm tube. This impaction might be due to a wandering of the aerosol stream from the center line of the chamber, while still remaining at the midplane of the chamber. Impaction could then occur because the aerosol stream would not be exactly lined up with the 1.3 mm tube.

## 7. Performance at high supersaturations

The data in this section show the results of varying the growth time available to nuclei experiencing large supersaturations in the chamber. The data in this section and the next were taken using room air as the test aerosol.

Fig. 7 shows results with the supersaturation held constant at 1%, the sample flow kept constant at 8.5 cm³ min⁻¹, and the flow into the optical counter kept constant at 0.4 ℓ min⁻¹. The total flow through the chamber was varied over the range 4–26 ℓ min⁻¹, as shown on the abscissa. The resulting concentrations of droplets larger than each of the five size thresholds of the optical counter are shown on the ordinate.

It can be seen from Fig. 7 that the concentration of droplets larger than 0.7 μm diameter or even 1.4 μm diameter is insensitive to total flow over the range 6 to 22 ℓ min⁻¹, corresponding to nucleus residence times in the chamber from 7 to 2 s, respectively. It can also be seen that the curves for the larger size thresholds asymptotically approach the plateau of the small size thresholds. Thus in going from 22 to 6 ℓ min⁻¹, the drops are growing, but the total number is staying constant; thus this number can be unambiguously defined to be the number of nuclei active at 1% supersaturation.

It can also be seen from Fig. 7 that at 10 ℓ min⁻¹ almost all the drops are smaller than 10 μm, whereas at 8 ℓ min⁻¹ almost all the drops are larger than this size. A similar result is seen for the 5 and the 3 μm thresholds, but the rise of the curves is not as steep, indicating that the droplets are less monodisperse for short growth times and smaller drop sizes.

Two other points to be made regarding Fig. 7 concern the left edge and the right edge of the plateau exhibited by the 0.7 and 1.4 μm thresholds. Regarding the left edge, the droplets are getting to be so large that they are impacting in the 1.3 mm tube leading to the optical counter. Further evidence of this impaction is given in Section 10. Regarding the right edge of the plateau, the count is decreasing because the residence

time in the chamber is too short for the combined processes of supersaturation rise in the chamber and nuclei growth to 0.7 $\mu$m diameter. At 26 $\ell$ min$^{-1}$ the residence time of the air passing through the chamber is only 1.6 s, which is very near the time required for the supersaturation to rise to its maximum value (Mahata *et al.*, 1973).

The experimental conditions for Fig. 8 are identical to those of Fig. 7, except that the supersaturation is 0.64%. These data would look very similar to those in Fig. 7, if they were plotted in the same way. Instead, however, we plotted the data as a histogram. The increasing monodispersity of the droplets as they grow larger is clearly seen.

## 8. Performance at low supersaturations

At low supersaturations it becomes more difficult to distinguish haze droplets from activated droplets. Indeed a significant fraction of the active droplets do not grow beyond their critical size in the chamber. In this situation the best one can do is estimate the maximum size of the haze droplets and then count all droplets larger than this as being droplets formed on active nuclei.

A haze droplet is one whose critical supersaturation $S_c$ is greater than the applied supersaturation $S$. Thus the haze droplet reaches an equilibrium size and then stops growing. For a given $S$, the largest haze droplet will be one with $S_c$ just above $S$. This haze droplet will have an equilibrium radius just below its critical radius $r_c$. Thus in operating a thermal diffusion chamber, all droplets larger than the $r_c$ corresponding to the operating $S$ should be counted as belonging to active nuclei. The question then arises as to whether one can predict this $r_c$ as a function of $S$ without knowing the chemical composition of the nuclei.

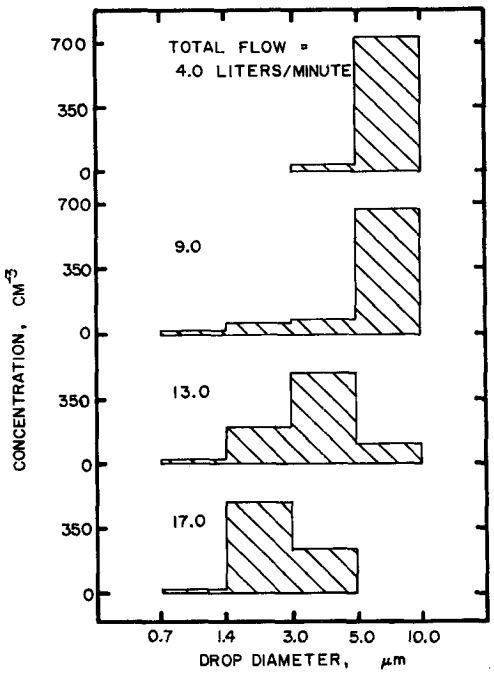


FIG. 8. Histogram size distributions. Supersaturation =0.64%. Other conditions as in Fig. 7.

Laktionov (1972) and Fitzgerald (1974) have shown that for most nuclei the relation between $S_c$ and the radius at 100% humidity ($r_{100}$) is only a weak function of either chemical composition or the fraction of insoluable material. This is an indication that at $r_{100}$, the insoluble portion of most nuclei is insignificant in volume compared to the volume of the water. Therefore, it will be even more insignificant when the nucleus has grown to $r_c$. Thus for most nuclei the relation between $r_{100}$ and $r_c$ for a pure solution droplet

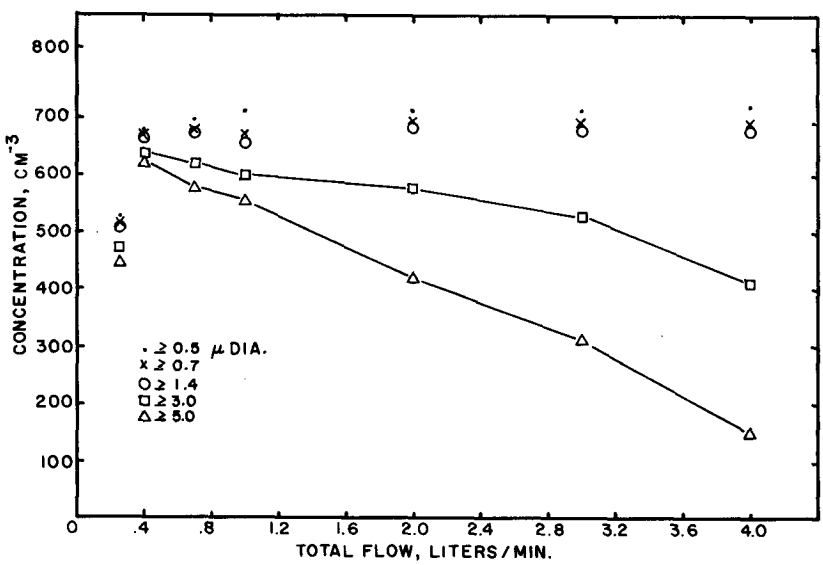


FIG. 9. As in Fig. 7 except at 0.14% supersaturation.

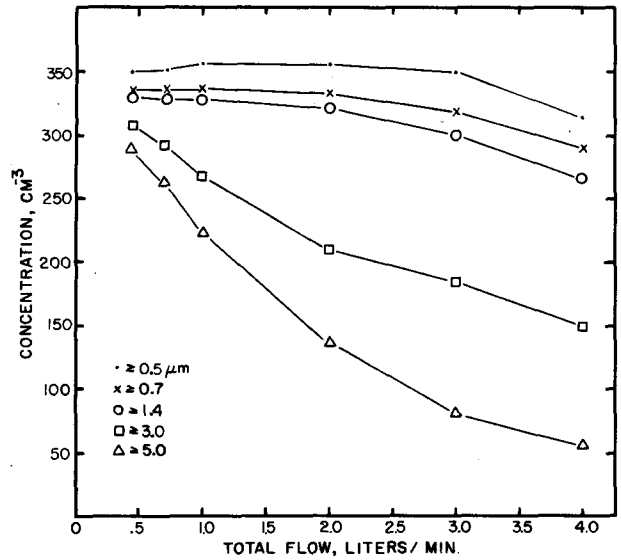


FIG. 10. As in Fig. 7 except at 0.08% supersaturation.

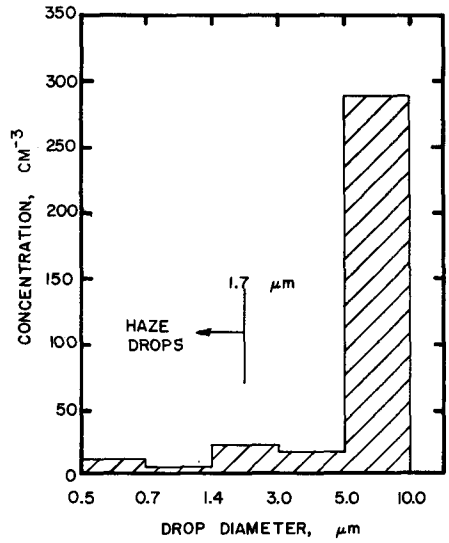


FIG. 11. Histogram size distribution at 0.08% supersaturation. Total flow = 0.4 $\ell$ min$^{-1}$.

should be valid. This relation is $r_c=\sqrt{3}r_{100}$ (Laktionov, 1972). Laktionov's relation between $r_{100}$ ($\mu$m) and $S_c$ (%) is $r_{100}=0.04\ S_c^{-1}$. Combining these two relations gives

$$r_c=0.069\ S_c^{-1}. \quad (2)$$

The experimental conditions for Fig. 9 are identical to those of Fig. 7, except that $S=0.14\%$. For this $S$, Eq. (2) indicates that all droplets >1.0 $\mu$m diameter should be counted as belonging to active nuclei. Referring to Fig. 9, it can be seen that at 0.4 $\ell$ min$^{-1}$, there are virtually no droplets in the size range 0.5–1.4 $\mu$m diameter. About 50 droplets cm$^{-3}$ are in the size range 1.4–5.0 $\mu$m diameter, but these are few as compared to the 600 droplets cm$^{-3}$ which are larger than 5.0 $\mu$m diameter. Since the largest haze droplet has a diameter of 1.0 $\mu$m, none of the droplets counted by the optical counter are haze droplets. There is no difficulty in distinguishing haze droplets from those grown on active nuclei.

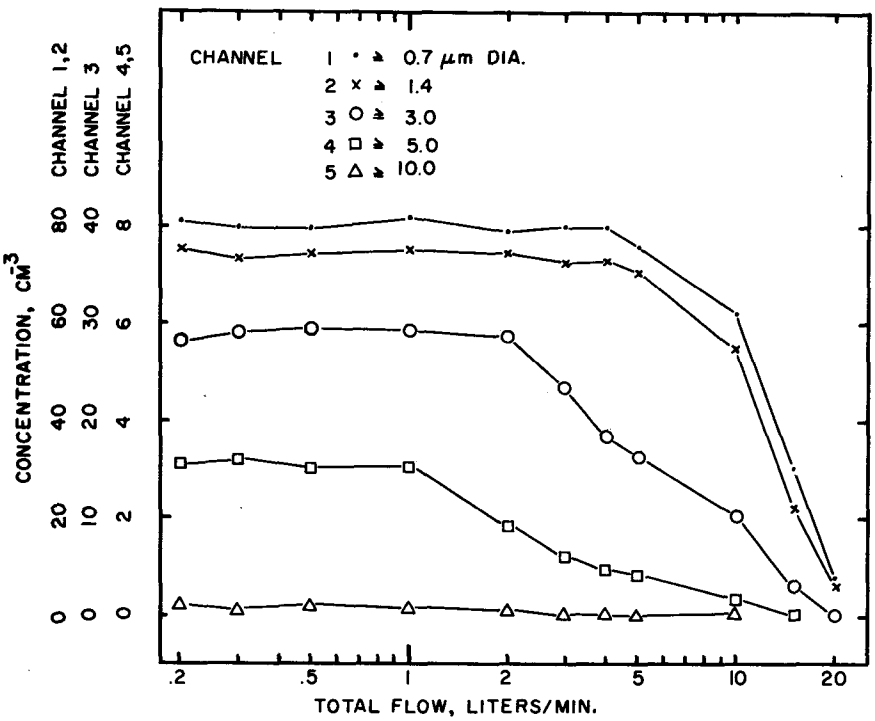


FIG. 12. Test in isothermal mode: Royco flow = 0.2 $\ell$ min$^{-1}$; sample flow = 8.5 cc min$^{-1}$.

Fig. 10 is the same as for Fig. 7 except for $S=0.08\%$. It can be seen that even at the lowest flow of 0.4 l min$^{-1}$, the drops are not monodisperse. To show this more clearly, the 0.4 $\ell$ min$^{-1}$ data are plotted as a histogram in Fig. 11. For this $S$, the maximum haze droplet is 1.7 $\mu$m diameter, and this is noted on Fig. 11. The concentration of droplets in the size range 0.5–1.7 $\mu$m diameter is about 40 cm$^{-3}$, whereas the number of drops larger than 1.7 $\mu$m diameter is about 310 cm$^{-3}$. Thus, about 13% of the drops being counted by the optical counter are haze droplets. We are now relying much more critically on the accuracy of the optical counter to size the droplets than we were at $S=0.14\%$ in Fig. 9. Likewise, we are critically relying on the accuracy of Eq. (2). In Laktionov's isothermal chamber, one also, relies upon the sizing accuracy of the optical counter and the relation between $r_{100}$ and $S_c$. Therefore, the thermal diffusion chamber performance at lower $S$ gradually evolves to that of an isothermal chamber.

## 9. Performance in the isothermal mode

The effect of evaporation in the Royco is the most critical problem when operating the chamber in the isothermal mode. This has already been discussed in Section 6. Two other tests of the isothermal performance are now presented.

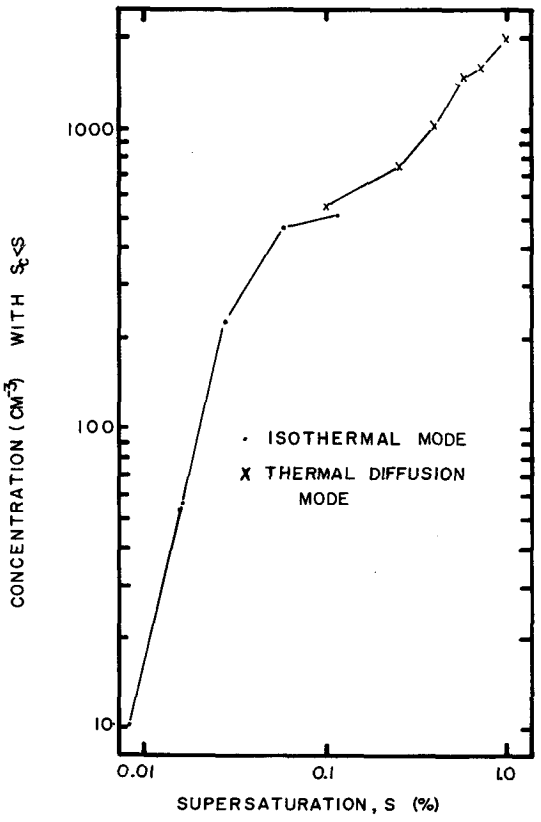


FIG. 13. Test of both modes on the same aerosol.

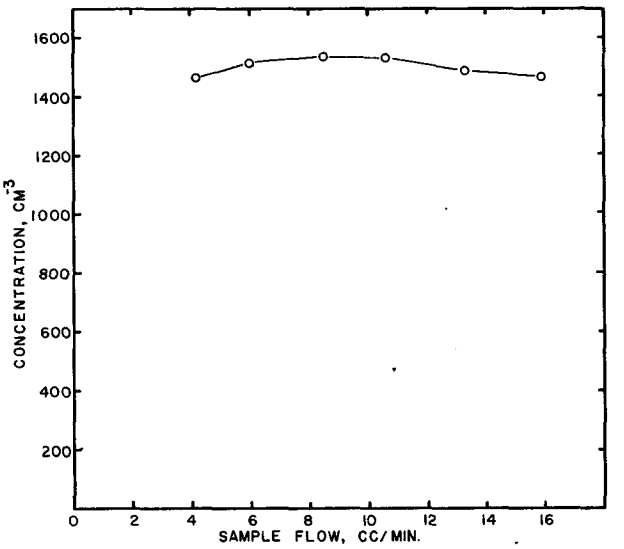


FIG. 14. Test of losses in chamber inlet tube. Supersaturation = 1%.

Fig. 12 shows the effect of varying the residence time when the chamber is operating in the isothermal mode. Room air stored in a 13 m$^3$ tank is the test aerosol. The chamber temperature is 27.5°C and the Royco bath temperature is 27.2°C. The sample flow is kept constant at 8.5 cm$^3$ min$^{-1}$, and the flow into the optical counter is held at 0.2 $\ell$ min$^{-1}$. It can be seen that as the total flow is decreased, the smaller size thresholds reach a plateau and then at lower total flow, the bigger size thresholds reach a plateau. This is because those nuclei with larger equilibrium radius take longer time to reach it.

The limitation on maximum growth time available in the isothermal mode is set by the lowest Royco flow, which is 0.2 $\ell$ min$^{-1}$. As explained in Section 6, the electronics in the optical counter starts to miss counting some of the droplets at flows below this. A flow of 0.2 $\ell$ min$^{-1}$ corresponds to a residence time in the chamber of about 200 s. According to the calculations of Laktionov (1972), it requires 180 s for a nucleus with $S=0.016\%$ to grow to within 5% of $r_{100}$. Here $r_{100}$ is 2.5 $\mu$m or 5 $\mu$m diameter; however, we point out that a nucleus with $S_c<0.016\%$ will grow to 5 $\mu$m diameter in less than 180 s. This may explain why the 5 $\mu$m threshold reaches a plateau in Fig. 12 at 1 $\ell$ min$^{-1}$ rather than at 0.2 $\ell$ min$^{-1}$. Presumably, it would occur at 0.2 $\ell$ min$^{-1}$ if we used monodisperse nuclei with $S_c=0.016\%$. On the basis of the maximum available growth time, we therefore take $S_c=0.016\%$ as the lower limit of our instrument. The upper limit of $S_c$ is set by evaporation effects in the Royco. As discussed in Section 6, in reference to Fig. 3, we take this to be $S_c=0.1\%$.

Fig. 13 shows results for testing the isothermal mode and the thermal diffusion mode using approximately the same aerosol. The data were taken over a 30 min period, using atmospheric air. It can be seen that the

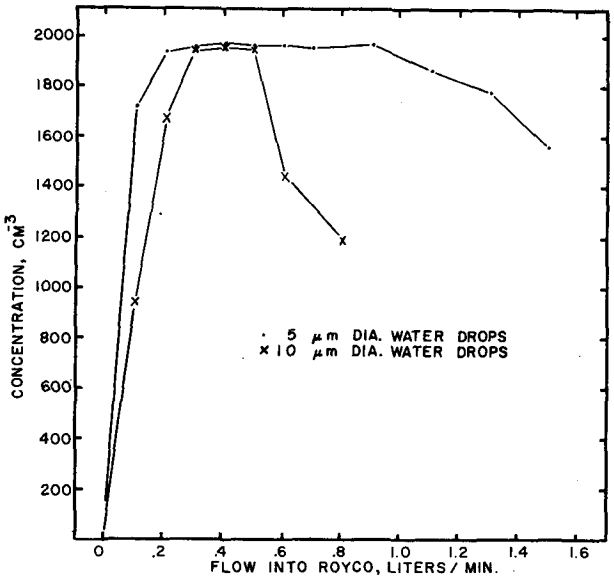


FIG. 15. Test of losses in Royco inlet tube for 10 and 5 μm diameter water drops.

two modes agree fairly well in the region where they very slightly overlap. To date about 50 spectra similar to Fig. 13 have been taken in an air sampling program which is underway. Most of the time the agreement between the two modes at $S=0.1\%$ is about as good as in Fig. 13. About 10% of the time, however, the disagreement gets as large as a factor of 2. This could be due to the fact that the aerosol is changing with time and we require about a half-hour to obtain the entire spectra.

## 10. Losses in chamber and Royco inlet tubes

Since nuclei with high $S_c$ diffuse more rapidly than larger nuclei, operation of the chamber at high supersaturation represents the worst case for diffusional losses in the sample metering tube. For $S=1\%$, Fig. 14 shows the influence of varying the sample flow through the sample metering tube. Room air was the test aerosol. It can be seen that the measured nucleus concentrations remained constant to within an accuracy of $\pm 2.5\%$, while the sample flow varied from 3 to 15 $cm^3$ $min^{-1}$. Thus diffusional losses in the sample metering tube are small.

Losses in the Royco inlet tube, if any, are expected to be by impaction, because the nuclei have grown to droplet size. Fig. 15 shows the results for varying the Royco flow, i.e., the flow through the 1.3 mm tube. The supersaturation is kept at 0.64%, the sample flow at 8.5 $cm^3 min^{-1}$. Two curves are shown, corresponding to total flows of 5 and 9 $\ell$ $min^{-1}$, both curves being made while using the same aerosol. The droplet diameter for the 5 $\ell$ $min^{-1}$ total flow is about 10 μm, whereas for the 9 $\ell$ $min^{-1}$ total flow it is 5 μm.

It can be seen in Fig. 15 that both curves exhibit a plateau, and that as the flow into the Royco increases the curves drop. The curve for the 10 μm droplets falls off more quickly than the curve for 5 μm droplets. This strongly suggests that the right edge of the plateaus is due to impaction. Presumably, this is because the aerosol stream is not lined up exactly with the 1.3 mm diameter tube. The drop at the left edge of the plateau is due to the fact that the electronics in the Royco fails to count some pulses at flow rates $<0.2$ $\ell$ $min^{-1}$, as discussed in Section 6.

## 11. Summary

A dual-range cloud nucleus counter is described and evaluated by experiment and calculations. In the isothermal mode of operation, nuclei with $0.016\% < S_c < 0.1\%$ can be counted and discriminated. The lower limit of $S_c$ is set by the maximum available growth time, which in turn is set by the minimum flow rate into the optical counter. The upper limit of $S_c$ is set by evaporation shrinkage of the smaller droplets as they pass into the optical counter. In order to reach this upper limit, the optical counter has to be thermostatted to within an accuracy of 0.1°C.

In the thermal diffusion mode of operation, nuclei with $0.1\% < S_c < 1.0\%$ can be counted and discriminated. The lower limit of $S_c$ is set by difficulty in discriminating haze drops from drops grown on active nuclei. Data taken at $S=0.08\%$ show that of the droplets with diameters between 0.5 and 10 μm, 83% are larger than 5 μm diameter, whereas the largest haze droplet is calculated to be 1.7 μm diameter. However, this interpretation depends upon the sizing accuracy of the optical counter, and upon approximation formulas which predict wet behavior of the nuclei without knowing nuclei chemical composition.

The two modes of operation do agree in the narrow region they overlap, i.e., near $S_c=0.1\%$.

*Acknowledgments.* Thanks are due to Dr. J. Carstens for help in performing the droplet shrinkage calculations, and to Dr. J. Podzimek, for use of the 13 $m^3$ aerosol storage tank.

This work was supported by the Atmospheric Sciences Section, National Science Foundation, under Grant NSF-ATM75-21421.

REFERENCES

Alofs, D. J., and J. Podzimek, 1974: A review of Laktionov's isothermal cloud nucleus counter. *J. Appl. Meteor*, **13**, 511–512.

——, and J. C. Carstens, 1976: Numerically simulated performance of widely used cloud nucleus counter. *J. Appl. Meteor.*, **15**, 350–354.

Fitzgerald, J. W., 1970: Non-steady-state supersaturations in thermal diffusion chambers. *J. Atmos. Sci.*, **27**, 70–72.

——, 1975: Approximate formulas for the equilibrium size of an aerosol particle as a function of its dry size and composition and the ambient relative humidity. *J. Appl. Meteor.*, **14**, 1044–1049.

Hoppel, W. A., and T. A. Wojciechowski, 1976: Accuracy limitations on CCN measurements with thermal gradient diffusion chambers. *J. Appl. Meteor.*, **15**, 107–112.

Hudson, J. G., and P. Squires, 1973: Evaluation of a recording continuous cloud nucleus counter. *J. Appl. Meteor*, **12**, 175–183.

——, and ——, 1976: An improved continuous flow diffusion cloud chamber. *J. Appl. Meteor.*, **15**, 776–782.

——, W. A. Hoppel, and T. A. Wojciechowski, 1977: A comparison of two CCN counters. *J. Appl. Meteor.*, **16**, 1120–1123.

Laktionov, A. G., 1965: Measurement of the concentration of cloud condensation nuclei. *Dokl. Akad. Nauk. SSSR*, **165**, 3–5.

——, 1968: Photoelectric measurements of condensation cloud nuclei. *J. Rech. Atmos.*, **3**, 63–70.

——, 1972: A constant temperature method of determining the concentrations of cloud condensation nuclei. *Atmos. Ocean Phys.*, **8**, 382–385.

Mahata, P. C., D. J. Alofs, and A. M. Sinnarwalla, 1973: Supersaturation development in a vertical-flow thermal diffusion chamber. *J. Appl. Meteor.*, **12**, 1379–1383.

Saxena, V. K., and J. C. Carstens, 1971: On the operation of cylindrical thermal diffusion cloud chambers. *J. Rech. Atmos.*, **5**, 11–23.

——, J. N. Burford and J. L. Kassner, Jr., 1970: Operation of a thermal diffusion chamber for measurements on cloud condensation nuclei. *J. Atmos. Sci.*, **27**, 73–80.

Sinnarwalla, A. M., and D. J. Alofs, 1973: A cloud nucleus counter with long available growth time. *J. Appl. Meteor.*, **12**, 831–835.

Squires, P., 1972: Diffusion chambers for measurement of cloud nuclei. *J. Rech. Atmos.*, **6**, 565–572.

Twomey, S., 1967: Remarks on the photographic counting of cloud nuclei. *J. Rech. Atmos.*, **3**, 85–90.